*J Mater Sci* (2016) 51:5061–5072

# Structural and morphological evolutions of spent FCC catalyst pellets toward NaA zeolite

M. R. Gonzalez[1], A. M. Pereyra[1,2], P. Bosch[3], G. Fetter[4], V. H. Lara[5], and E. I. Basaldella[1,*]

[1] *Centro de Investigación y Desarrollo en Ciencias Aplicadas Dr. J.J. Ronco (CINDECA) (CONICET-CIC-UNLP), 47 N° 257, B1900 AJK La Plata, Argentina*

[2] *Centro de Investigación y Desarrollo en Ciencia y Tecnología de Materiales (CITEMA), Universidad Tecnológica Nacional, 60 y 124, 1900 La Plata, Argentina*

[3] *Instituto de Investigaciones en Materiales, Universidad Nacional Autónoma de México, Ciudad Universitaria, Circuito Exterior, 04510 Mexico, DF, Mexico*

[4] *Facultad de Ciencias Químicas, Benemérita Universidad Autónoma de Puebla, Ciudad Universitaria, Blvd. 14b Sur y Avenida San Claudio, 75520 Puebla, PUE, Mexico*

[5] *Universidad Autónoma Metropolitana-Iztapalapa, Avenida San Rafael Atlixco 186, 09340 Mexico, DF, Mexico*

**Received:** 26 October 2015
**Accepted:** 3 February 2016
**Published online:** 16 February 2016



## ABSTRACT

Spherically shaped pellets, usually discarded after use in fluidized-bed catalytic cracking units (FCCs), were converted to zeolite A-surface-enriched pellets. The final pellets were obtained through a two-step treatment consisting of: (1) alkaline thermal activation followed by (2) a hydrothermal crystallization in selected reaction conditions. The alkaline thermal activation provided pellets mainly constituted by silico-aluminate compounds. When the pellets are heated at 800 °C in contact with sodium carbonate, a structural rearrangement occurs which includes nepheline, crystalline aluminosilicate, and an amorphous fraction expected to be silicon-enriched, preserving the pellet original geometry. Afterward, reaction mixtures were prepared by adding sodium hydroxide solution to the heat-treated product. Then, commercial sodium aluminate was added. During the hydrothermal synthesis at 85 ± 3 °C, zeolite A was formed from the calcined product and $NaAlSiO_4$ turned out to be an intermediary crystalline compound. The LTA crystals were already observed for a reaction time of 0.5 h, but the highest conversion to pure zeolite A was reached after 6 h. Those final round solid pellets showed an external surface fully covered by well anchored zeolite A cubic crystals about 1–2 μm in size. Such materials may be very useful in ion exchange, molecular sieving, and adsorption processes. The crystalline ordering was followed by XRD, SEM, NMR, and water adsorption.

Address correspondence to E-mail: eib@quimica.unlp.edu.ar

DOI 10.1007/s10853-016-9809-7

## Introduction

The discovery and synthesis of zeolites have boosted chemical technology since the 1940s. These synthetic or natural aluminosilicates are molecular sieves regular porous structure of which can accommodate a wide variety of cations. Due to these features, zeolites are used to tackle catalytic and adsorptive challenges in the oil industry. In particular, zeolite-based catalysts are used in the fluid catalytic cracking (FCC) units to convert petroleum crude oils to more valuable gasoline, olefinic gases, and other products. The modern FCC units are continuous processes that operate 24 h a day for as long as 2–3 years between scheduled shutdowns for routine maintenance [1]. A FCC unit processing 75,000 barrels per day (11,900 $m^3$/day) circulates about 55,900 metric tons of catalyst per day. Only in Argentina, 360 tons of waste catalysts per cracking unit are annually generated. Conventionally, these wastes are mainly disposed as landfills [2, 3].

The main components of the FCC catalysts nowadays in use are crystalline synthetic zeolite (15–50 wt%), an aluminosiliceous matrix (ca. 5 wt%), binder (ca. 20 wt%, usually Ludox) and kaolin clay (60–25 wt%). The zeolite present in FCC catalysts corresponds to the Y type (FAU group), usually fully hydrogen exchanged (USY).

The chemical composition of spent FCC catalysts turns out to be 50 % of $SiO_2$ and 45 % of $Al_2O_3$; the remaining 5 % is distributed among other minor components [4]. Therefore, waste FCC catalysts seem to be an adequate starting material for the synthesis of zeolite A, and its formula is $Na_{96}Al_{96}Si_{96}O_{384}(H_2O)_{216}$, characterized by an atomic Si:Al ratio of 1. Zeolite A, also known as Linde type A, pertains to the LTA structural group, and is one of the most synthesized zeolites. Its main uses include ion exchange, molecular sieving, and water adsorption in industrial processes. Starting materials may be kaolin [5, 6], sodium silicate and sodium aluminate [7], metakaolin [8–10], or powder glass [11], among others.

In previous works, it was found that the exhausted FCC catalyst is an adequate source to be used to synthesize zeolite A [12, 13]. The synthesis of zeolite A was optimized in such a way that the catalyst calcined at 800 °C using 50 wt% of sodium carbonate as alkaline activator resulted in the best conversion to zeolite [13]. It was also demonstrated that aqueous solutions containing low concentrations of chromium (III) could be purified by ion exchange using the zeolitized product [14]. However, the process of the conversion to zeolite A has not been carefully followed and no intermediate compounds have been reported. Matters as important as how fast is the zeolite formation or how different are the first crystalline products from those of the final material, remain open.

Thus, the purpose of this work is to study the structural and morphological evolution of the microspheroidal catalyst particles during the hydrothermal synthesis of zeolite A. The intermediate compounds formed during the synthesis are characterized to provide a reaction scheme based on physicochemical parameters. The synthesis mechanism is followed through the radial distribution function (X-ray diffraction, XRD) and by changes in the coordination of the aluminum atoms that are Al IV in zeolite, but Al V in alumina (Nuclear magnetic resonance, NMR). Additionally, textural evolution is studied by water adsorption. The morphology of the resulting products is observed by scanning electron microscopy (SEM), being the chemical composition determined by energy dispersive X-ray spectrometry (EDS).

## Experimental

### Materials

#### *Waste catalyst sample*

A spent fluid bed cracking catalyst provided by a commercial unit was used for this study. The chemical analysis of the catalyst proved to be (wt%): $SiO_2 = 49.5$, $Al_2O_3 = 45.1$, $Na_2O = 1.4$, $Fe_2O_3 = 1.7$, $TiO_2 = 1.0$, $La_2O_3 = 0.5$, $P_2O_5 = 0.5$, and other metal oxides: 0.2. As FCC particles could be broken in smaller pieces or become smaller in size by attrition, the size fraction between 100 and 60 μm was selected by screening (sample named 4090-0).

### Hydrothermal synthesis

The procedure was similar to the methodology detailed in [12]. Briefly, a mixture of the discarded catalyst (sample 4090-0) and $Na_2CO_3$ (Baker, analytic degree) containing 50 wt% of catalyst was prepared under sonication. After 5 min of mixing, the solid

was activated by calcination under static conditions at 800 ± 10 °C, for 2 h. Hydrothermal crystallization was performed at 85 ± 3 °C, in closed vessels. Reaction mixtures were prepared by adding a 4 M aqueous NaOH solution to the heat-treated product, with stirring at room temperature. Then, commercial sodium aluminate was added (36.5 % $Al_2O_3$, 29.6 % $Na_2O$, 33.9 % $H_2O$), in a molar proportion ($NaAlO_2$/NaOH) of 0.026. This mixture was aged for 24 h at room temperature, without stirring. The alkaline solution added at the beginning of the reaction was prepared to reach a starting molar ratio $Na_2O/Al_2O_3 = 2{:}1$, which is favorable to obtain NaA zeolite as main product [15, 16]. The mixtures enclosed into 250 ml polypropylene reactors were heated to 85 ± 3 °C, maintaining constant stirring. Samples were taken at representative reaction times, 0 min (4090-1), 15 min (sample 4090-3), 30 min (sample 4090-4), 5 h (4090-16), and 6 h (4090-F). In each withdrawal, the solid sample was separated from the liquid phase by centrifugation, washed and dried at 110 °C.

## Characterization methods

### *X-ray diffraction*

To identify the crystalline compounds, a Siemens D500 PW powder diffractometer coupled to a copper anode tube was used to obtain the XRD patterns. The Cu-Kα radiation was selected with a diffracted beam monochromator. The amounts of amorphous and crystalline phases were estimated from the corresponding areas of the diffractograms. No calibration curve was required as aluminum, silicon, and sodium have rather similar scattering factors and compositions [17].

Radial distribution function or pair correlation function in a system of particles (atoms, molecules, colloids, etc.), describes how density varies as a function of distance from a reference particle. Such density variations may be interpreted as the most probable interatomic distances. From XRD patterns obtained using a molybdenum anode X-ray tube coupled to a Siemens D500 PW powder diffractometer, those distributions may be obtained. The $K_\alpha$ radiation was selected with a filter. Intensity data, measured by step scanning with a scintillation counter, were the input to the Radiale program [18].

### *Nuclear magnetic resonance*

Nuclear magnetic resonance (NMR) was chosen to determine the coordination number of aluminum atoms that is 4 in zeolite, but 5 in alumina. Nuclear magnetic resonance (NMR) measurements were performed in a Bruker Avance 400 Spectrometer. The spectrometer was operated at a resonance frequency of 79.50 and 104.27 MHz for $^{29}$Si and $^{27}$Al MAS. Spectra were recorded after single $\pi/2$ excitation with repetition times of 5 and 7 μs for Si and Al, respectively. Samples were spun at 7.5 and 10 kHz (aluminum) and 5 kHz (silicon), and the chemical shifts were referenced to TMS. Furthermore, the Si:Al ratio can be calculated from the intensities of the different signals $I_{Si(nAl)}$, according to

$$\frac{Si}{Al} = \frac{\sum_{n=0}^{4} I_{Si(nAl)}}{\sum_{n=0}^{4} 0.25 n I_{Si(nAl)}}$$

where n is the number of aluminum atoms bonded to tetrahedral silicon $(SiO_4)^{4-}$, and $I$ is the intensity of the peaks of NMR spectra [19]

### *Water adsorption*

Although the conventional estimations of specific surface areas are performed using nitrogen, in this study, we selected water as adsorbent. Indeed, nitrogen molecules are too large to diffuse into the zeolite A pores whereas water molecules are known to access to all the zeolite porosity [20]. The surface area of zeolite-containing samples was evaluated from adsorption–desorption isotherms in the BET range of relative water vapor pressure, using the Brunauer–Emmett–Teller (BET) method [21, 22]. The first step in the application of the BET method is to obtain the monolayer capacity ($N_m$) from the BET plot. The second step is to calculate the surface area $S$ from the equation $S = N_m M^{-1} L \omega$, where $L$ is the Avogadro number ($6.02 \times 10^{23}$), $M$ is the molecular weight of water (gram per mole) and $\omega$ is the molecule cross-sectional area ($10.8 \times 10^{-20}$ m$^2$ for water molecule). If $N_m$ is expressed in grams of adsorbate (water) per gram of solid, the specific surface area $S$ (m$^2$ g$^{-1}$) is estimated from the monolayer capacity as $S = 3612\, N_m$.

### *Scanning electron microscopy and energy dispersive X-ray spectrometry*

Particle size and morphology were observed by scanning electron microscopy (SEM). The semiquantitative chemical analysis aimed at estimating aluminum and silicon contents was carried out by energy dispersive X-ray spectrometry (EDS). A JEOL JSM-7600F (Field Scanning Electron Microscope) coupled to an EDS Oxford INCAX-Act was used. Note that the samples were not sputtered with any conductor material to avoid any further contribution to the EDS spectra.

## Results

## XRD analyses

### *Compounds*

The reference sample (4090-0), i.e., the spent FCC catalyst elemental composition of which was given in the introduction section, contained crystalline Y type zeolite and an amorphous phase [12]. Conventional XRD patterns of samples 4090-0, 4090-1, 4090-3, 4090-4, and 4090-F are compared in Fig. 1. The starting material, i.e., sample 4090-1, was the sample taken from the reactor at time zero; it contained $NaAlSiO_4$, which had crystallized as a low amount of nepheline (PDF# 19-1176) and as a crystalline sodium aluminosilicate (PDF# 11-0221) i.e., low carnegieite, both are minerals which belong to the group of nepheline, sodalite and carnegieite, all feldspathoids with a molar ratio of Si:Al:Na. They differ on their atomic order. Both nepheline and carnegieite (mentioned as "crystalline sodium aluminosilicate" in this work) have ring structures; still an amorphous fraction expected to be silicon-enriched is present.

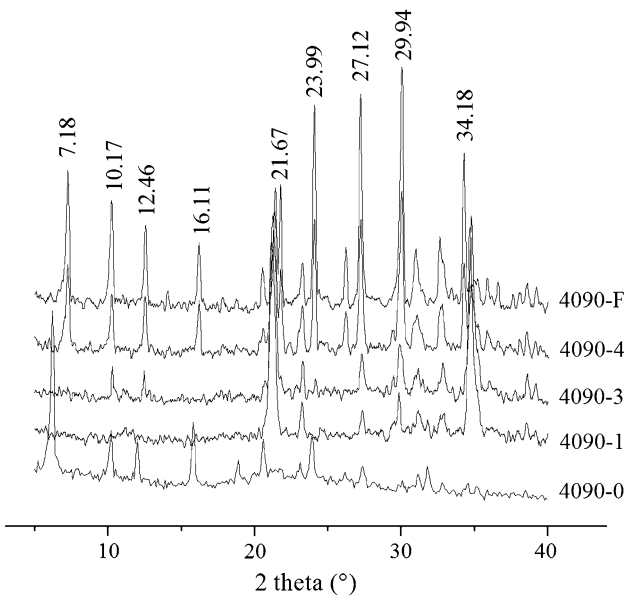


**Figure 1** X-ray diffraction patterns of samples 4090-0, 4090-1, 4090-3, 4090-4, and 4090-F. The initial crystalline sodium aluminosilicate is progressively transformed to zeolite A.

In sample 4090-3, small peaks at $2\theta = 10.1°$ and 12.4° could be attributed to zeolite A, which turned out to be the main component of samples, 4090-4 and 4090-F. Sample 4090-4 presents only zeolite A and a small fraction of amorphous compound (26 %) similar to the one observed in the initial material (27 %). In the same way, nepheline content remains constant during the whole process (<15 %). Sample 4090-F was the less amorphous (22 %) and contained the highest amount of zeolite A; still, very small amounts of hydroxysodalite, with the formula, $Na_6Al_6Si_6O_{24}$ $Na_2(OH)_2(H_2O_2)$, could be inferred by the very low-intensity peaks at $2\theta = 14°$ and 35°, less than ca. 4 %. In Fig. 1, the zeolite A peak intensities increase with reaction time, and simultaneously, the peaks corresponding to the crystalline sodium aluminosilicate (low carnegieite) diminish. Figure 2 shows an XRD quantification of the evolution of the zeolite A and the crystalline sodium aluminosilicate content during the hydrothermal reaction. Zeolite A seems to be formed from the crystalline sodium aluminosilicate as the amorphous compound percentage remains almost constant (22–27 %).

### *Structure*

The radial distribution functions of samples, 4090-1 and 4090-3 (Fig. 3), present a radial distribution function first peak at $r = 1.6$ Å and a second one at $r = 3.1$ Å. The first one can be attributed to the interatomic distance (Si, Al)–O (under our experimental conditions, the distances Si–O = 1.60 Å and Al–O = 1.75 Å could not be resolved) and the second one to (Si, Al)–(Si, Al) [17, 23, 24]. This second peak presents a shoulder at $r = 2.7$ Å that corresponds to the O–O and/or Na–O distance. The peak at $r = 4.05$ Å is due to the interatomic distance between (Si, Al) and O as second neighbors.

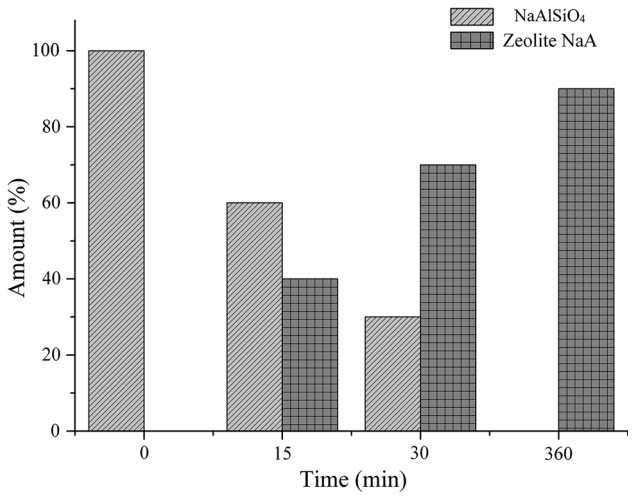


**Figure 2** Relative percentages of zeolite A and crystalline sodium aluminosilicate, both referred to the total amount of crystalline phase as a function of reaction time.

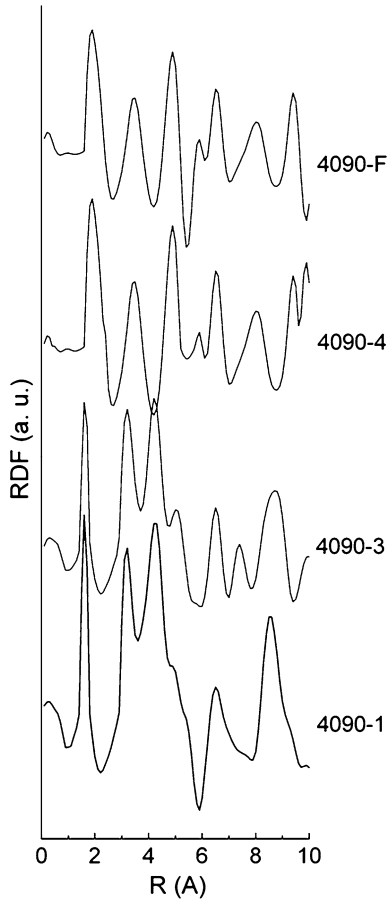


**Figure 3** Radial distribution functions of samples 4090-1, 4090-3, 4090-4, and 4090-F.

If the radial distribution functions of samples, 4090-3 and 4090-4, are compared, the differences are clear. They have to be attributed to the fact that one sample (4090-3) contains $NaAlSiO_4$ as main component and the other (4090-4) is composed mainly of zeolite A. Both present a small fraction of amorphous compound. The first peak, in sample 4090-4, is located at $r = 1.75$ Å, and the shift of this peak toward higher values could be correlated with the presence of aluminum in tetrahedral coordination; the obtained value agrees with the value already reported in the literature [25, 26]. The following peak was found at $r = 3.5$ Å (sample 4090-4) and, as in the other samples, it corresponds to a (Si, Al)-(Si, Al) distance. The next peak appears at 4.95 Å, which is probably due to (Si, Al)-O (second neighbors). The radial distribution function of the sample, 4090-F, reproduces the features of sample, 4090-4. It must be noted that the radial distribution functions correspond to the full samples; therefore, they include interatomic distances of all compounds present in each material.

From the first peaks of the radial distribution function, distances (Si, Al)–O and (Al, Si)–(Si, Al), as given in Table 1, and the angle between (Si, Al) tetrahedra may be evaluated (Fig. 4). For simplicity, in this figure, the central atom of the tetrahedron is labeled Si, but it corresponds to Si or Al. Of course, the Al–Al bond is forbidden by the Lowenstein rule [15].

In samples, 4090-1 and 4090-3, the angle turned out to be 176° and in samples, 4090-4 and 4090-F, it was180°. Therefore, the oxygen tetrahedra assembly was reorganized until it became linear, as expected in a cubic structure (zeolite A). Note that if the angle was calculated for the distance (Si, Al)–(Si, Al) = 2.7 Å which was the shoulder of the radial distribution function, it corresponds to 116°. Such value may be due to the atomic network of the noncrystalline compound observed in conventional XRD patterns.

Some of the obtained interatomic distances were in agreement with those already reported for other aluminosilicates [27]; the measured angles between tetrahedra in zeolite A and the sample, 4090-F, however, differed from those of Tait [28] (155.2°–156.9°) due to the precursor reactants as well as the amorphous compound previously mentioned but mainly because the synthesized zeolite is A type.

**Table 1** X-ray diffraction results: correlations between the interatomic distances and the identified compounds (csa = crystalline sodium aluminosilicate or ZA = zeolite A)

| Samples | Identified compounds | Radial distribution function | | | | |
|---|---|---|---|---|---|---|
| | | First peak (Si, Al)–O (Å) | Shoulder O–O or (Si, Al)–Si (Å) | Second peak (Si, Al)–Si (Å) | Third peak Si–O (Å) | Si–O–Si angle |
| 4090-1 | csa | 1.6 | 2.7 | 3.1 | 4.05 | 176° |
| 4090-3 | csa + ZA[a] | 1.6 | 2.7 | 3.1 | 4.05 | 176° |
| 4090-4 | ZA + csa[a] | 1.75 | – | 3.5 | 4.95 | 180° |
| 4090-F | ZA | 1.75 | – | 3.5 | 4.95 | 180° |

[a] Small amount

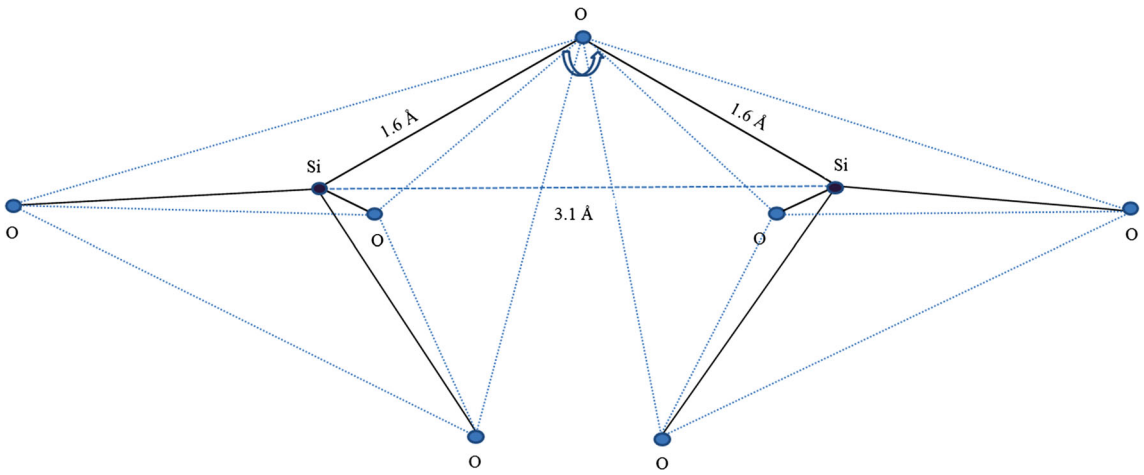


**Figure 4** Angle between (Si, Al)–$O_4$ tetrahedra in samples 4090-1 and 4090-3 with (Si, Al)–(Al, Si) bond distance of 3.1 Å.

## NMR Studies

### *Environment of Si and Al Atoms*

$NaAlSiO_4$ is known to present four well-defined peaks: at −85.1 ppm attributed to Si(4Al), at −88.4 ppm attributed to Si(4Al), at −91.4 ppm attributed to Si(3Al), and at −101.8 ppm attributed to Si(0Al), with the peak at −85.1 ppm being the most intense [29]. The $^{29}$Si NMR spectrum of kaolin usually presents a unique peak at −91.4 ppm corresponding to Si(1Al) [30]; during dehydroxylation, the Si atoms present different environments with distortion, the line then broadens due to variations in the Si–O–Si(Al) bond angles [8]. Zeolite A is characterized by an intense peak at −89 ppm, but if some X zeolite is present, a small peak at −85.3 appears [7]. The peak at −71.3 is usually attributed to silicate with Si(0Al) [7]. In this context, the interpretation of the obtained NMR spectra is straightforward. Indeed, the $^{29}$Si-MAS spectrum of sample 4090-0 shows a broad peak with three maxima, the first two at −78 and −83 ppm (the most intense), attributed to Si(3Al) and Si(4Al), respectively, and, the third, at −89 ppm corresponding to Si(3Al) and Si(4Al) species, Table 2 [31, 32].

The peak initially in −83 ppm also decreases up to a relative intensity of 12 % in the sample 4090-F. This peak Si(4Al) may be attributed to the initial zeolite Y, to nepheline, or to zeolite A. Instead, the peak at −89 ppm, corresponding to Si(4Al) (assigned to zeolite Y in sample 4090-0, to nepheline or/and a crystalline aluminosilicate in sample 4090-3 and to zeolite A in samples, 4090-4 and 4090-F), increases with synthesis time in agreement with previous works [7, 33, 34]. In samples, 4090-1 and 4090-3, this peak was very broad revealing a wide range of environments due to distortions of the Si–O–Si(Al) bond angles. In samples, 4090-4 and 4090-F, the peak

**Table 2** NMR characteristic peaks in ppm corresponding to nepheline and/or the crystalline aluminosilicate (*), zeolite A (+), amorphous silicate (x), and zeolite Y (°) for $^{29}$Si and $^{27}$Al

| Samples | Si(4Al) | Si(3Al) and Si(4Al) | Si(3Al) and Si(4Al) | $Al(O–Si)_4$ |
|---|---|---|---|---|
| 4090-0 | −88.9 (60 %)° | −83.9 (100 %)° | −77.7 (50 %)$^{x}$ | 59° |
| 4090-1 | −88.9 (80 %)* | −82.5 (100 %)* | −78 (50 %)$^{x}$ | 59* |
| 4090-3 | −89.3 (100 %)$^{+}$ | −83.2 (50 %)$^{*,+}$ | −78 (20 %)$^{x}$ | 59* |
| 4090-4 | −89.6 (100 %)$^{+}$ | −83.9 (12 %)$^{*,+}$ | −78 (2 %)$^{x}$ | 58$^{+}$ |
| 4090-F | −89.6 (100 %)$^{+}$ | −83.2 (12 %)$^{+}$ | – | 58$^{+}$ |

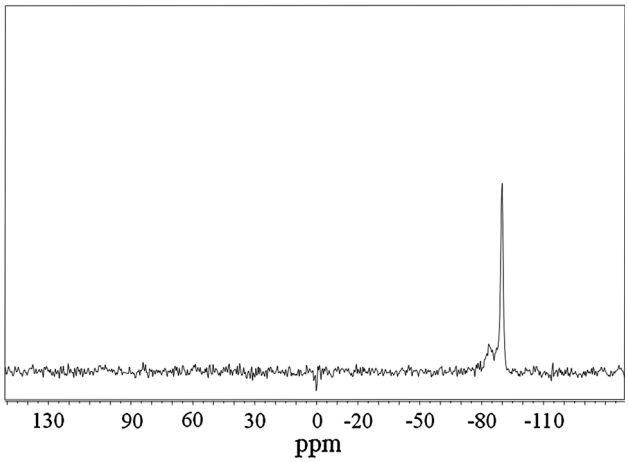


**Figure 5** NMR spectrum for $^{29}$Si at 5000 Hz: sample 4090-F.

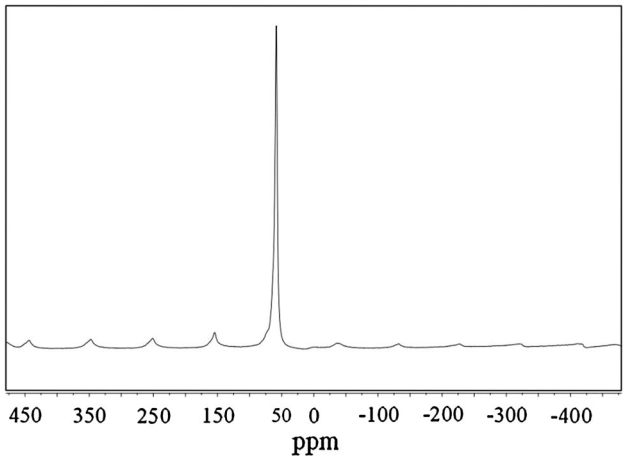


**Figure 6** NMR spectra for $^{27}$Al at 10000 Hz; sample 4090-F.

Si(4Al) became significantly more intense and narrow showing that the zeolite crystallinity and crystallite size have increased [7, 34, 35]. The $^{29}$Si-MAS spectrum of sample 4090-F is presented in Fig. 5. Note that not only the peak at −89 ppm is detected, but a small peak at −85.3 is present showing that some zeolite X is also synthesized.

The $^{27}$Al-MAS spectra complemented and corroborated the $^{29}$Si-MAS results. The $^{27}$Al spectrum of the waste catalyst, sample 4090-0, showed a very intense peak at 59 ppm attributed to a four-coordinated aluminum species linked to silicon atoms via bridging oxygen atoms, $Al(O–Si)_4$, chemical shift of which is characteristic of aluminum in crystalline Y zeolite [35].

In samples, 4090-1 and 4090-3, this peak (59 ppm) appeared at the same chemical shift, which is due to the presence of nepheline and the crystalline aluminosilicate, but it is shifted to 58 ppm in the spectra of samples, 4090-4 and 4090-F, which corresponds to the chemical shift value expected in zeolite A [36]. The $^{27}$Al-MAS spectra of the sample 4090-F are presented in Fig. 6. NMR results are, then, in agreement with the previously presented XRD results: zeolite A appears as the crystalline sodium aluminosilicate disappears with reaction time.

## Specific surface area

The specific surface areas were determined by water adsorption (Table 3). The specific surface area of the spent catalyst (4090-0) was 156 $m^2/g$. Sample, 4090-16, which corresponds to a reaction time of 5 h, is included.

At the beginning of the reaction, the specific surface area diminished from 202 $m^2/g$ (sample 4090-1) to 134 $m^2/g$ (sample 4090-4), i.e., by 35 %. This initial diminution of specific surface area with treatment time shows that either the sodium crystalline aluminosilicate is first decomposed in a material of low specific area, and then this material forms the zeolite A, or that the pores of the formed zeolite A are occluded and are not accessible to water. Such discontinuities or "humps" in the growing zeolite features have been reported previously and have been attributed to an 'autocatalytic nucleation' model of zeolite crystallization also supporting the hypothesis about the presence of inhomogeneous nuclei distribution into gel phase [37].

Specific surface area then increases regularly with synthesis time. It increased up to 314 (4090-16) and 681 $m^2/g$ (4090-F), Table 3. Note that with this

technique, the last steps of zeolite A crystallization are differentiated. Indeed, as the crystalline aluminosilicate (its surface area must be small compared to zeolite A) disappears, zeolite A is formed.

**Table 3** Specific surface areas as determined by water adsorption

| Sample | Synthesis features | Specific surface area ($m^2/g$) |
|---|---|---|
| 4090-0 | Waste catalyst | 156 |
| 4090-1 | Starting material | 202 |
| 4090-3 | 15 min | – |
| 4090-4 | 30 min | 134 |
| 4090-16 | 5 h | 314 |
| 4090-F | Final | 681 |

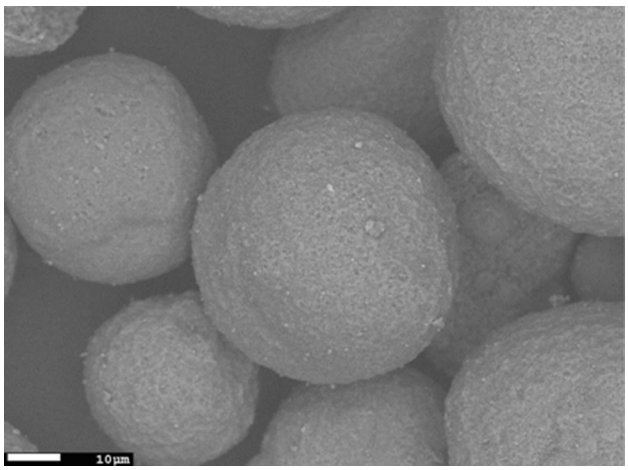


**Figure 7** SEM micrograph of the exhausted FCC catalyst, 4090-0. *Bar* 10 µm.

## Morphology

The morphology and particle size of the reaction products were observed via scanning electron microscopy, macroscopically (low magnification) and microscopically (high magnification). SEM micrographs clearly show that the hydrothermally synthesized products maintain the pellet morphology of the starting catalyst even after a reaction time of 6 h, the obtained pellet diameter was similar to the diameter of the pellet of the original cracking catalyst, ca. 60–100 µm (Fig. 7).

After being aged for 24 h at room temperature (sample 4090-1), the pellets show a surface covered by needle-shaped crystals which are identified as the crystalline aluminosilicate by the XRD results, Fig. 8a. At a higher magnification, Fig. 8b, the crystals of zeolite A, globularly shaped ($d = 0.8$ µm), begin to grow on the pellet surface. As the reaction proceeds (samples 4090-4 and 4090-F), Fig. 9, the pellet surface is increasingly transformed in cubically shaped crystals, typical of zeolite A. The average size of the crystals in sample 4090-F is $d = 1.2$ µm, the size distribution is rather homogeneous, and no more needle-shaped particles are observed. Note how the zeolite crystals emerge from the pellet surface, samples 4090-4, and 4090-F, Fig. 9. In sample 4090-4, the zeolite A presents two crystal sizes, a larger one which is of ca. $d = 1.0$ µm, and a large amount of smaller ones of ca. 0.3 µm.

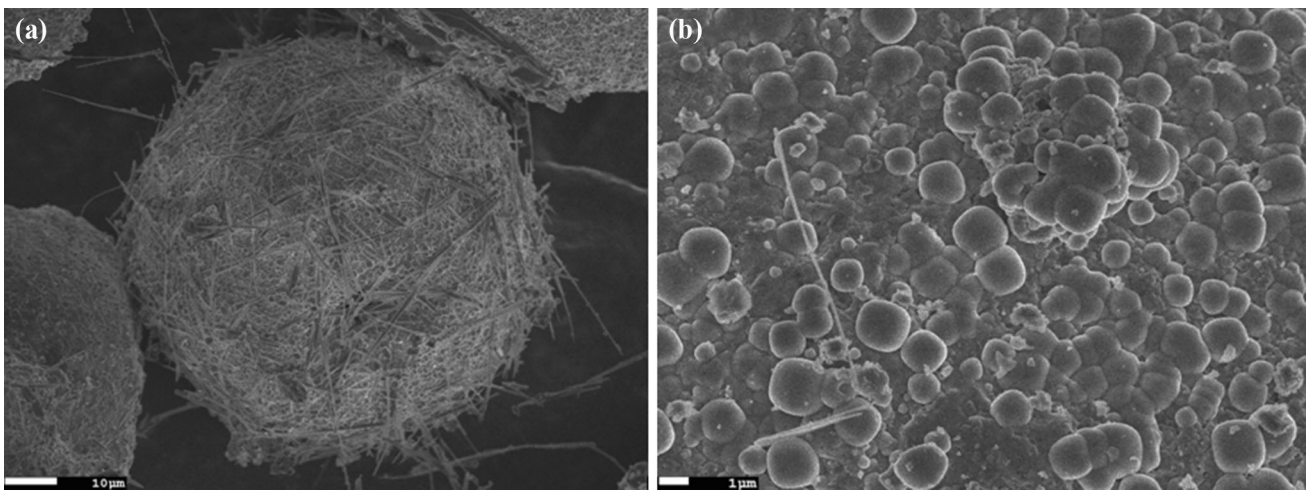


**Figure 8** SEM micrographs of sample 4090-1 at two different magnifications. **a** *Bar* 10 µm, **b** *Bar* 1 µm.

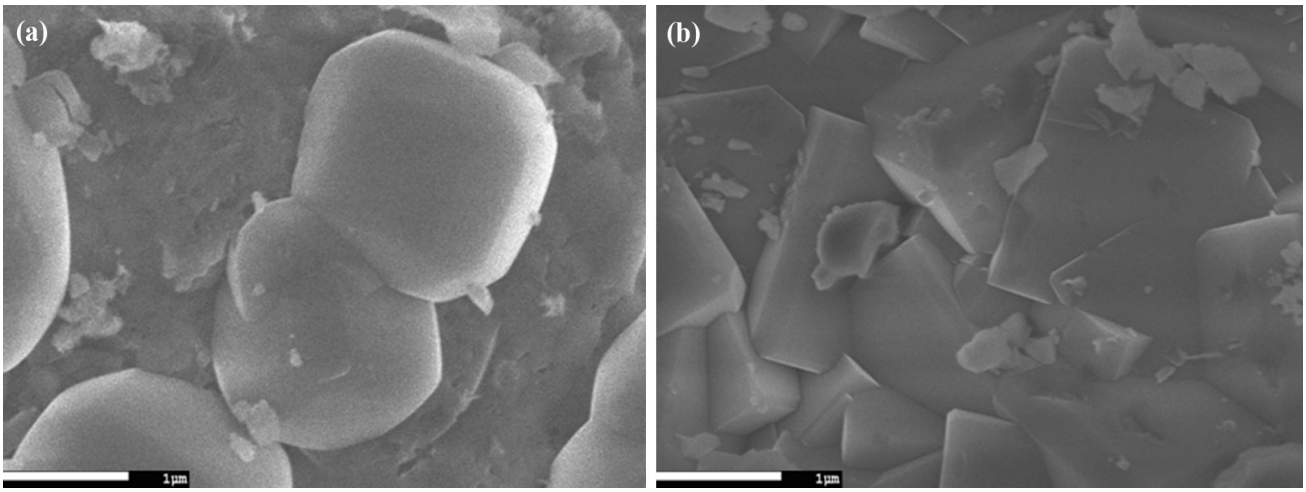


**Figure 9** Comparison of the SEM micrographs of **a** sample 4090-4 (*bar* 1 μm) and **b** 4090-F (*bar* 1 μm).

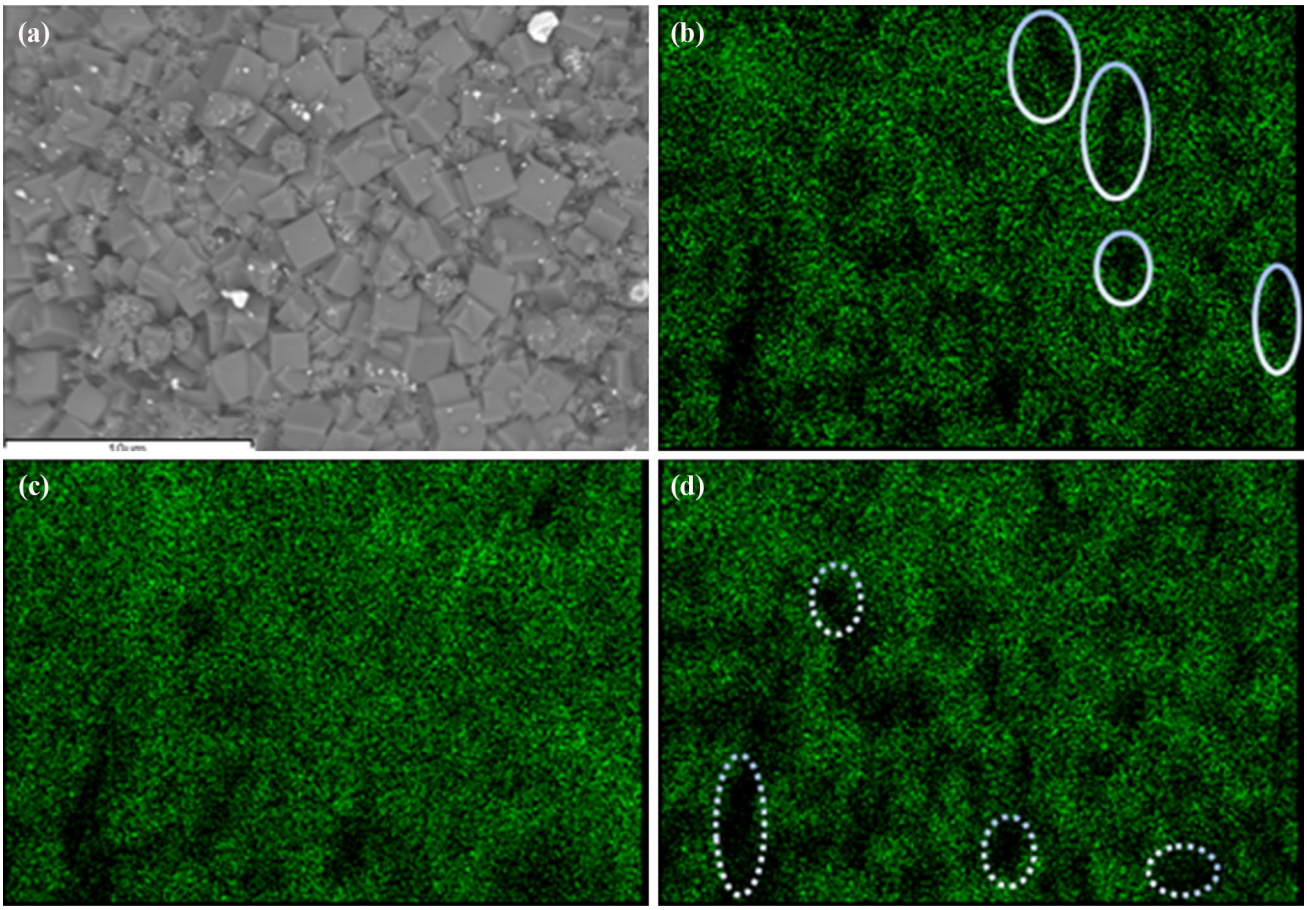


**Figure 10** SEM-EDX analyses for sample 4090-F, showing the same selected area in the four pictures. *Bar* 10 μm. **a** SEM micrograph, **b**, **c**, and **d** Aluminum, silicon, and sodium EDX mapping corresponding to the micrograph shown in **a**, respectively.

## Elemental composition

The EDS analysis of sample 4090-1 confirms that the Si:Al ratio = 1.46 should provide zeolite A with $SiO_2$ in excess. This analysis is interesting as it corresponds to a layer of 2–3 μm which is the depth at which the electrons penetrate. Hence, as zeolite A composition guarantees a Si:Al = 1, the small growing crystals could be supported on a Si-enriched amorphous compound which may correspond to the amorphous silicate already reported in the X-ray Diffraction and Nuclear Magnetic Resonance sections. As reaction time increases (samples 4090-4 and 4090-F), the Si:Al ratio is maintained as expected. Still some nickel is observed in all analyses. It has to be attributed to residual heavy metals which are often incorporated during the cracking process.

As the previous analyses are local, a mapping of Si and Al is presented for 4090-F, Fig. 10. Silicon is found all over the sample surface, whereas aluminum is missing in some selected areas as shown in the figure with continuous circles, Fig. 10b, c. Those small regions must correspond to the unreacted catalyst surface which is enriched with silica, and they can be correlated to the underlying very small particles observed in the micrograph, Fig. 10a. The surfaces where both elements (Al and Si) are present match with the sodium map of Fig. 10d. They can be associated to the image cubes attributed to zeolite A. The zones encircled with a broken line, which do not correspond to silicon or to aluminum or to sodium and appear dark in all mappings, can be explained as an experimental artifact. Indeed, rough samples which present different levels tend to absorb the emitted X-rays. Geometric effects due to surface roughness can impact X-ray generation and propagation sufficiently to result in relative intensity contributions of a factor as high as ten in severe cases [38].

## Discussion

Our results may be summarized as follows. Macroscopically, the spherically shaped pellets are fully covered by zeolite A at a reaction time as small as 30 min (sample 4090-4), in which sample the zeolite particle edges are smoothed. As expected, the zeolite crystals grow and turn out to be cubic with sharp edges with reaction time (sample 4090-F).

Microscopically, the synthesis follows two sequential steps: first, the crystalline aluminosilicate is formed, and then the crystalline aluminosilicate generates zeolite A; still, small fractions of nepheline and the amorphous compound initially present in the catalyst do not react. In the first step, i.e., the calcination of the catalyst at 800 °C in the presence of $Na_2CO_3$, nepheline and a crystalline sodium aluminosilicate are obtained as has been often reported earlier [27, 39]. However, the transformation of the crystalline aluminosilicate to zeolite A (second step) implies the reordering of the hexagonal network of this compound to the cubic lattice of zeolite A. Both compounds present 8-ring windows with size of 3.7 × 4.8 $Å^2$ in carnegieite and 4.1 × 4.1 $Å^2$ in zeolite A [40].

The early stages of nucleation of zeolite A are dominated by four ring species as shown by theoretical studies [41]. However, in our study, the initially synthesized crystalline sodium aluminosilicate provides other building units. In this reaction, the geometry of the 8-ring windows evolves with time as crystalline sodium aluminosilicate collapses and zeolite A appears. Such transformation can only be due to the synthesis conditions which have a high hydration rate and a very high pH value. The collapse of crystal lattice is commonly described as a loss of long-range order, which manifests, in radial distribution functions, as peak fading for high r values. Sample 4090-1 did not show this feature. Therefore, conversion of crystalline sodium aluminosilicate to zeolite A takes place by direct solid–solid topotactic transformation. The dehydrated crystalline sodium aluminosilicate in the presence of high amounts of water is transformed directly at low temperature to cubic zeolite A. The initial pH value is revealed by the rounded edges of the zeolite A formed in sample 4090-3. Indeed, such morphology is obtained after a controlled nucleation period and increased redissolving due to the high alkalinity of the mixture after crystallization [42].

Besides, Si:Al ratio obtained by NMR presents similar values compared to those obtained by EDS analysis. For sample 4090-1, the Si:Al ratio is greater than 1, and this value guarantees the synthesis of zeolite A with $SiO_2$ in excess. As reaction time increases, for the samples 4090-4 and 4090-F, the Si:Al ratio turns out to be 1, which value confirms the presence of zeolite A.

Simultaneously, the specific surface area increased with reaction time as zeolite A appears, excluding sample 4090-4 with the specific surface area of ca. 33 % being lower than the starting material. As zeolite A is already observed, the topotactic transformation of

crystalline sodium aluminosilicate has started. The corresponding expected surface area was much higher than the measured one. Therefore, a fraction of the total surface must be inaccessible to water adsorption. Zeolite A crystallite surface must be covered by a nanometric layer of an amorphous compound beyond the resolution of scanning electron microscopy.

## Conclusions

Zeolite A could be efficiently synthesized from waste FCC catalysts via a rather simple process. Such methodology opened an important window to the use of exhausted catalysts produced by the oil industry. The crystallization of zeolite A was followed by complementary techniques such as XRD, NMR, and water adsorption. The results showed that the progressive structural modifications were due to the network ordering. First, a crystalline sodium aluminosilicate is synthesized as an intermediary compound to give rise to zeolite A, which, as time goes on, may partially redissolve due to the very high alkalinity. Increased crystallinity was observed as the surface of the spherical particles was progressively covered with zeolitic crystals. The final zeolite A on top of the pellets turns out to be fully crystalline with a clear cubic morphology. In this sense, the obtained solid is the most valuable material as it may prove to be a good industrial adsorbent.

## Acknowledgements

The NMR technical work of Gerardo Cedillo is gratefully recognized. As well, the technical works by Adriana Tejeda and Omar Novelo are acknowledged in respect of XRD and SEM–EDS, respectively. The authors offer their thanks to A. Ermili for performing experiments. M. R. Gonzalez thanks CONICET and BECAR Argentina for scholarship funding.

## References

[1] Cejka J, Corma A, Zones S (2010) Zeolites and catalysis. Wiley, Federal Republic of Germany

[2] Al-Jabri K, Baawain M, Taha R, Al-kamyani ZS, Al-Shamsi K, Ishtieh A (2013) Potential use of FCC spent catalyst as partial replacement of cement or sand in cement mortars. Constr Build Mater 39:77–81

[3] Morozov Y, Castela AS, Dias APS, Montemor MF (2013) Chloride-induced corrosion behavior of reinforcing steel in spent fluid cracking catalyst modified mortars. Cem Concr Res 47:1–7

[4] Basaldella EI, Paladino JC, Solari M, Valle GM (2006) Exhausted fluid catalytic cracking catalysts as raw materials for zeolite synthesis. Appl Catal B 66:186–191

[5] Johnson EBG, Arshad SE, Asik J (2014) Hydrothermal synthesis of zeolite A using natural kaolin from KG. gading bongawan sabah. J Appl Sci 23:3282–3287

[6] Wang J, Huang Y, Pan Y, Mi J (2014) Hydrothermal synthesis of high purity zeolite A from natural kaolin without calcination. Microporous Mesoporous Mater 199:50–56

[7] Shi J, Anderson MW (1996) Direct observation of zeolite A synthesis by in situ solid-state NMR. Chem Mater 8:369–375

[8] Chandrasekhar J (1996) Influence of metakaolinization temperature on the formation of zeolite 4A from kaolin. Clay Miner 31:253–261

[9] Maia AAB, Neves RF, Angélica RS, Pöllmann H (2015) Synthesis, optimisation and characterisation of the zeolite NaA using kaolin waste from the Amazon Region. Production of Zeolites KA, MgA and CaA. Appl Clay Sci 108:55–60

[10] Ayele L, Pérez-Pariente J, Chebude Y, Díaz I (2015) Synthesis of zeolite A from Ethiopian kaolin. Microporous Mesoporous Mater 215:29–36

[11] Vinaches P, Rebitski EP, Alves JABRL, Melo DMA, Pergher SBC (2015) Unconventional silica source employment in zeolite synthesis: raw powder glass in MFI synthesis case study. Mater Lett 159:233–236

[12] Basaldella EI, Torres Sánchez RM, Conconi MS (2009) Conversion of exhausted fluid cracking catalysts into zeolites by alkaline fusion. Appl Clay Sci 42:611–614

[13] Gonzalez MR, Pereyra AM, Basaldella EI (2011) Trivalent chromium ion removal from aqueous solutions using low-cost zeolitic materials obtained fron exhausted FCC catalyst. Adsorpt Sci Techol 29:629–636

[14] Gonzalez MR, Pereyra AM, Torres Sánchez RM, Basaldella EI (2013) Chromium removal by zeolite-rich materials obtained from an exhausted FCC catalyst: Influence of chromium incorporation on the sorbent structure. J Colloid Interf Sci 408:21–24

[15] Breck DW (1974) Zeolite molecular sieves: structure, chemistry, and use. Wiley, New York

[16] Bosch P, Ortiz L, Schifter I (1983) Synthesis of faujasite type zeolites from calcined kaolins. Ind Eng Prod Res Dev 22:401–406

[17] Klug HP, Alexander LE (1974) X-ray diffraction procedures for polycrystalline and amorphous materials. Wiley, New York

[18] Magini M, Cabrini A (1972) Programme en FORTRAN IV pour l'analyse des données expérimentales relatives à la diffusion des rayons X par des substances liquides, amorphes et microcristallisées. J Appl Cryst 5:14–18

[19] Klinowski J, Thomas JM, Fyfe CA, Gobbi GC (1982) Monitoring of structural changes accompanying ultrastabilization of faujasitic zeolite catalysts. Nature 296:533–536

[20] Gorbach A, Stegmaier M, Eigenberger G (2004) Measurement and modeling of water vapor adsorption on zeolite 4A-equilibria and kinetics. Adsorption 10:29–46

[21] Gregg SJ, Sing KSW (1978) Adsorption, surface area, and porosity. Academic Press, London

[22] Torres Sánchez R, Falasca S (2007) Specific surface area and surface charges of some Argentinian soils. Z Pflanz Bodenk 160:223–226

[23] Gutiérrez G (2002) Atomistic simulation of densified amorphous alumina. Rev Mex Fis 3:60–62

[24] Song MK, Chon H (1993) Structural transition of A-type zeolite molecular dynamics study. Bull Korean Chem Soc 14:255–262

[25] Leonard AJ, Ratnasamy P, Declerck D, Fripiat JJ (1971) Structure and properties of amorphous silico-aluminas Part 5.—Nature and properties of silico-alumina surfaces. Discuss Faraday Soc 52:98–108

[26] Aguilar-Pliego J, Bosch P, Zicovich-Wilson C, Herrera-Pérez G, Lara VH (2012) On three-fold coordinated Si sites in mesoporous MCM-41 catalysts. Open Catal J 5:50–55

[27] Dimitrijevic R, Dondur V, Vulic P, Markovic S, Macura S (2004) Structural characterization of pure Na-nephelines synthesized by zeolite conversion route. J Phys Chem Solids 65:1623–1633

[28] Tait KT, Sokolova E, Hawthorne FC, Khomyakov AP (2003) The crystal chemistry of nepheline. Can Miner 41:61–70

[29] Stebbins JF, Murdoch JB, Carmicael ISE, Pines A (1986) Defects and short-range order in nepheline group minerals: a silicon-29 nuclear magnetic resonance study. Phys Chem Miner 13:371–381

[30] Watanabe T, Shimizu H, Nagasawa K, Masuda A, Saito H (1987) 29Si and 27Al-MAS/NMR study of the thermal transformations of kaolinite. Clay Miner 22:37–48

[31] Engelhardt G, Fahlke B, Mägi M, Lippmaa E (1983) High-resolution solid-state 29Si and 27Al n.m.r. of aluminosilicate intermediates in zeolite A synthesis. Zeolites 3:292–294

[32] Stöker M (1996) Characterization of zeolitic materials by solid-state NMR-state of the art. Stud Surf Sci Catal 102:141–189

[33] Radulovic A, Dondur V, Vulic P, Miladinovic Z, Ciric-Marjanovic G, Dimitrijevic R (2013) Routes of synthesis of nepheline-type polymorphs: an influence of Na-LTA bulk composition on its thermal transformations. J Phys Chem Solids 74:1212–1220

[34] Tabernero V, Camejo C, Terreros P, Alba MD, Cuenca T (2010) Silicoaluminates as "Support Activator" systems in olefin polymerization processes. Materials 3:1015–1030

[35] Engelhardt G, Michel D (1987) High-resolution solid-state NMR of silicates and zeolites. Wiley, Norwich

[36] Freude D, Fröhlich T, Pfeifer H, Scheler G (1983) N.M.R. studies of aluminium in zeolites. Zeolites 3:171–177

[37] Miladinovic Z, Zakrzewska J, Kovacevic B, Bacic G (2007) Monitoring of crystallization processes during synthesis of zeolite A by in situ 27 Al NMR spectroscopy. Mater Chem Phys 104:384–389

[38] Newbury DE, Ritchie NWM (2013) Quantitative SEM/EDS, step 1: what constitutes a sufficiently flat specimen? Microsc Microanal 19(Supplement 2):1244–1245

[39] Ohgushi T, Ishimaru K (2001) Nepheline and carnegieite ceramics from A zeolites by microwave heating. J Am Ceram Soc 84:321–327

[40] Baerlocher CH, McCusker LB, Olson DH (2007) Atlas of zeolite framework types, 6th edn. IZA-SC Publications, Elsevier

[41] Yang CS, Mora-Fonz JM, Catlow CRA (2013) Modeling the nucleation of zeolite A. J Phys Chem C117:24796–24803

[42] Kurzendörfer CP, Kuhm P, Steber J (1996) Zeolites in the environment. In: Schwuger MJ (ed) Surfactants science series, vol 65. Marcel Dekker, New York